High Deposition Rate Aluminium Doped Zinc Oxide Films with Highly Efficient Light Trapping for Silicon Thin Film Solar Cells

S. Calnan [1,2], J. Hüpkes [2], B. Rech [2], H. Siekmann [2], A. N. Tiwari [1]

[1]Loughborough University, Department of Electronic and Electrical Engineering, Centre of Renewable Energy Systems Technology, Loughborough, United Kingdom
[2]Institute of Photovoltaics, Research Centre Jülich, Germany

Abstract

Aluminium doped zinc oxide films were deposited on glass substrates at high rates by reactive mid frequency sputtering. The in-line sputter system allows oxygen influx along the middle and sides of a dual cathode system. The effect of varying the oxygen flow from the sides on the electrical and optical properties together with the surface morphology after wet chemical etching was investigated. Increasing the amount of oxygen flow from the sides improved the resistivity profile of static prints and gave highly conductive and transparent films in dynamic deposition mode. The etched films developed rough surface textures with effective light scattering which could be controlled by the oxygen balance between the middle and sides. Optimally textured films were used as front contacts in 1cm² single junction µc-Si:H solar cells yielding an initial efficiency of 8.4 %. The improvement in light trapping lead to short circuit densities higher than that of the reference solar cells.

1. Introduction

Zinc oxide is gaining importance as a transparent contact for thin film silicon solar cells [see for example 1 - 9]. Compared to fluorine doped tin oxide (SnO_2:F), which is commonly used in commercial production, zinc oxide is resistant to hydrogen rich plasmas used for chemical vapour deposition of thin film silicon layers. Aluminium doped zinc oxide (ZnO:Al) also has better transparency and conductivity than commercial SnO_2:F coated glass substrates [1].

An additional function of the front contacts in superstrate pin solar cells, is the improvement of performance by efficient light trapping. This requires the front contact to have a suitably rough surface to scatter the light under high angles into the silicon. By repeated total internal reflection within the silicon, the effective light path is strongly enhanced, leading to significant absorption of long wavelength light, though the corresponding absorption coefficient of silicon is quite low. Zinc oxide can either directly grow with a rough surface [see for instance, 2,3] or is roughened after sputter deposition through wet chemical etching [4]. The latter technique is used in this study for films deposited by reactive medium frequency (MF) magnetron sputtering.

Presently, state of the art ZnO:Al films with excellent resistivity, transparency and a surface morphology suitable for light trapping are routinely deposited in our laboratory using RF magnetron sputtering from ceramic targets. However, for industrial scale production of ZnO:Al, reactive magnetron sputtering from metallic Zn:Al targets is more attractive owing to the higher deposition rate, cheaper target material and easier scalability to larger areas [10]. MF reactive sputtering has been proven to produce high quality ZnO:Al films at high deposition rates. Though the application of such ZnO:Al films as front contacts silicon thin film solar cells lead to high efficiency [7 - 9], more work needs to be done to improve the quality of the surface morphology after etching. This work therefore focused on improving the properties of MF sputtered ZnO:Al films with the goal that their performance in solar cells at least matches the current state of the art ZnO:Al films obtained by RF sputtering from ceramic targets [6].

2. Experimental Details

Substrates measuring 10 x 10 cm² were used to allow co-deposition on up to nine 0.7 mm thick pieces of Corning 1737 glass in a vertical inline sputter system (VISS 300 manufactured by von Ardenne Anlagentechnik GmbH, Germany). The ZnO:Al films were deposited by mid frequency (40kHz) reactive magnetron sputtering from two Zn/Al (99.5/ 0.5 wt%) targets on a dual cathode system. The size of each target was 10 x 75 cm². The chamber was evacuated to a base pressure of 10^{-5} Pa. Argon, used as sputter gas, enters the process chamber via two manifolds along the outer sides of the cathode system. The principal inlet for oxygen is a manifold situated between the two targets facing the substrate. The process was stabilised at a fixed working point in the transition region by adjusting the oxygen flow using Plasma Emission Monitoring PEM® [11]. The PEM intensity is typically in the range from 20 % to 50% [8]. Low PEM intensity indicates oxidic deposition, while 50% corresponds to the metallic mode. The choice of working point was important as it has been found to have a considerable effect on the properties of the ZnO:Al films [9, 10].

For this study, a fixed portion of oxygen was channelled via the argon manifolds so that the oxygen distribution is more homogeneous over the cathode system. Then the process was controlled by varying only the quantity of additional oxygen from the central inlet required to maintain a stable working point.

Several sets of films were deposited using different proportions of the two oxygen inlet configurations. The details of the deposition conditions of the films are summarised in Table 1. Relatively low process pressures were chosen as it has been established that such ZnO:Al films are more suitable for solar cells [12] and more stable to damp-heat conditions [13].

Table 1
Summary of deposition parameters, discharge power P, total process pressure p_{tot} , substrate temperature T_s, PEM intensity and oxygen flow rate F_O from the outer sides. The middle oxygen flow varied in the range of 34 - 42 sccm and 70 - 121 sccm for low and high power, respectively

Film	P [kW]	p_{tot} [Pa]	T_s [°C]	F_O [sccm]	PEM [%]
A1	10	1.8	330	0	35
A2	10	1.8	330	200	35
B1	4	0.11	310	60	30
B2	4	0.11	310	60	32.5
B3	4	0.11	310	60	35
B4	4	0.11	310	70	35
B5	4	0.11	310	80	35
C1	10	0.5	310	100	25
C2	10	0.5	310	100	27.5
C3	10	0.5	310	100	30
C4	10	0.5	310	150	30
C5	10	0.5	310	200	30
C6	10	0.5	310	250	30
C7	10	0.5	310	270	32.5

The sheet resistance R_s, of the films was measured using either the four-point or two-point method depending on the size of film area in consideration. A Dektak 3030 stylus profiler (by Veeco Instruments) was used to measure the film thickness d, which was used together with R_s to determine the resistivity ρ of the films. Carrier mobility μ, and carrier density N, of the films were determined by the van der Pauw Hall method at room temperature using a Keithley 926 system.

All films deposited were smooth and had to be etched using 0.5% diluted hydrochloric acid to obtain a suitable surface morphology for light scattering. A Lambda 19 spectrometer (Perkin Elmer) was used to measure the optical properties of the etched films over the 300-1300nm wavelength range. The total transmittance T and reflectance R were measured, using di-iodomethane (CH_2I_2) as an index matching fluid to eliminate errors by light trapping within the ZnO:Al film. T and R spectra were used to determine the absorbance A. The haze ratio of the etched films was determined as the fraction of diffuse (scattering angles exceeding 5°) transmittance making up the total transmittance.

Selected films were used as substrates for microcrystalline silicon (μc-Si:H) thin film solar cells with a 1.1 μm thick intrinsic absorber layer. Details of cell preparation are described elsewhere [5,6]. Solar cell characteristics were measured using a sun simulator (Wacom- WXS-140S-Super) at standard test conditions (AM 1.5, 100mW/cm² at 25°C). The differential spectral response (DSR), at zero bias, of some solar cells was also measured and used to obtain the external quantum efficiency.

3 Results and Discussion

3.1 Statically deposited films

Two films deposited in stationary mode under identical conditions except for oxygen inlet configuration, were compared (see table 1). Film A1 was deposited with oxygen inlet from the middle only and for A2, additional oxygen was added from the outer gas inlet. Thickness and resistivity profiles of both films are shown in Figure 1. The thickness profile of film A2 was considerably more uniform but slightly lower as compared to film A1.

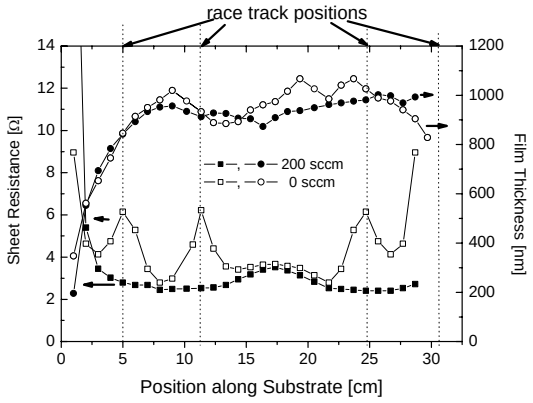

Fig. 1. Sheet resistance (squares) and thickness (circles) of statically deposited ZnO:Al films as a function of position along the substrate. Film A1 with oxygen flow from the middle only is represented by unfilled shapes and film A2 with oxygen from both the middle and the sides of the targets by solid shapes.

Sheet resistance was about 3 Ω for both films but peaked to about 6 Ω for film A1 at the positions on the substrate facing the racetracks of the targets. These peaks were significantly diminished in film A2 giving a lower and more homogeneous sheet resistance profile. The resistivity of films A2 and A1 deviated from the mean value by ± 10.6% and ± 23.9 %, respectively, along the length of the substrate.

3.2 Electrical Properties of Dynamically Deposited Films

Figure 2 illustrates the dependence of resistivity on oxygen distribution for dynamically deposited films. Considering films B3 to B5, (see Table 1 for deposition details), an increase in the oxygen flow F_O through the outer inlet, from 60 to 80 sccm caused the resistivity to slightly rise from 3.5 x 10^{-4} Ω cm to 4.0 x 10^{-4} Ω cm. To check, if this effect is caused by a possibly different working point, though the PEM intensity was kept constant, films B1 to B3 (see Table 1) were prepared at different working points with F_O fixed at 60 sccm. The intentional shift of working

point by a slight reduction of PEM intensity from 35 % over 32.5% to 30% causes a larger rise in ρ from 3.5 x 10^{-4} Ω cm over 4.1x 10^{-4} Ω cm to 5.0x 10^{-4} Ω cm. Similar results were obtained for films C1 to C7, which are also included in Figure 2.

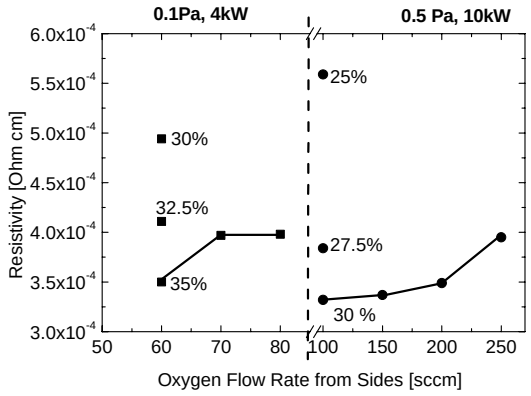

Fig. 2. Resistivity as a function of F_O. Squares and circles represent film types B and C, respectively. The percentage values represent the applied PEM intensity. The lines are to guide the eye. Refer to Table 1 for details.

The slight rise in resistivity with increase of F_O is mainly caused by a slight decrease in carrier density of the films as can be seen in figure 3. For instance, for films B3 to B5, the carrier density stays nearly constant around 4.9 x 10^{20} cm^{-3} when F_O was increased from 60 to 80 sccm. Considering films C3 to C6, the carrier density decreased slightly from 4.9 x 10^{20} cm^{-3} to 4.5 x 10^{20} cm^{-3} as parallel oxygen flow increased from 100 to 250 sccm. On the whole, a slight reduction in PEM intensity resulted in large reductions of carrier density.

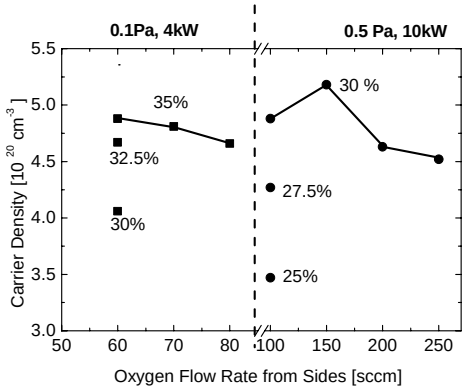

Fig. 3. Carrier density as a function of oxygen flow rate parallel to the substrate surface. Squares and circles represent film types B and C respectively. See Table 1 for details. Note: the lines are to guide the eye.

The carrier mobility of films B3 to B5 reduces from 8 cm^2/Vs to 35 cm^2/Vs as F_O is increased from 60 sccm to 80 sccm though it remains higher than if the PEM intensity had been reduced (see left side of Figure 4). Similarly considering films C3 to C6, the mobility generally slightly reduces from 37 cm^2/Vs to 36 cm^2/Vs for F_O between 100 and 250 sccm though there is an abrupt increase to 39 cm^2/Vs at F_O = 200 sccm. It should be noted that the variations of N and μ are still within the error of the Hall measurement about 10% making qualitative inference very difficult. All the same, the tendency of resistivity to reduce with increasing F_O indicates a reduction of both N and μ.

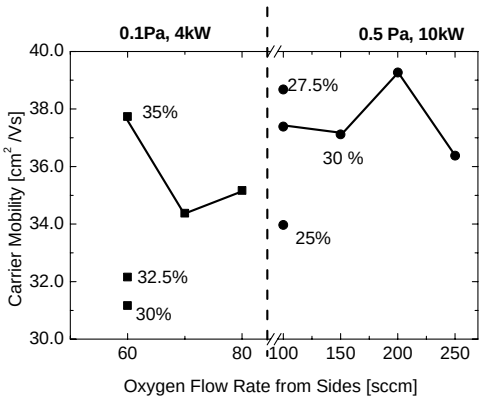

Fig. 4. Carrier mobility as a function of F_O. Squares and circles represent film types B and C, respectively. See Table 1 for details. Note: the lines are to guide the eye.

In summary, the mobility and carrier density of the ZnO:Al films are only slightly affected by increasing the oxygen flow F_O, but tend to decrease, which results in slight increases in film resistivity. The comparison with the shift of the PEM intensity indicates that the working point is at most slightly affected by the different oxygen distribution at constant PEM intensity.

3.3 Textured Films

Since the as-deposited films are smooth, we etched all of them in 0.5% hydrochloric acid for various time intervals in order to roughen their surfaces for strong light scattering. Initially, all films in series B and C were etched for 30 seconds to compare the resulting surface texture. In general, the etch rate of the ZnO:Al films increased with F_O at constant PEM intensity from 2.5nm/s to 3.5 nm/s and from 3 nm/s to 7.8 nm/s for films B3 to B5 and C3 to C6, respectively. In both cases, the increase in etch rate with F_O is much less than if the working point is slightly shifted closer to the oxide mode. The moderate etch rates obtained demonstrate the relative ease of adjusting the etched film behaviour by varying the oxygen flow from the sides.

3.3.1 Etched Film Structure

Scanning Electron Microscopy was used to study the surface morphology of the etched films. Figures 5 a) and b) show SEM images of the surface of a state of the art RF sputtered ZnO:Al film after etching for 5s and 40s (optimised), respectively. It can be seen from figure 5b) that the surface of the optimised film is well distributed with wide bottomed craters of diameters around 1μm. A previous study has indeed demonstrated that these features are well suited to good light trapping ability in solar cells

[6]. Therefore, this type of film was subsequently used as a reference for this work.

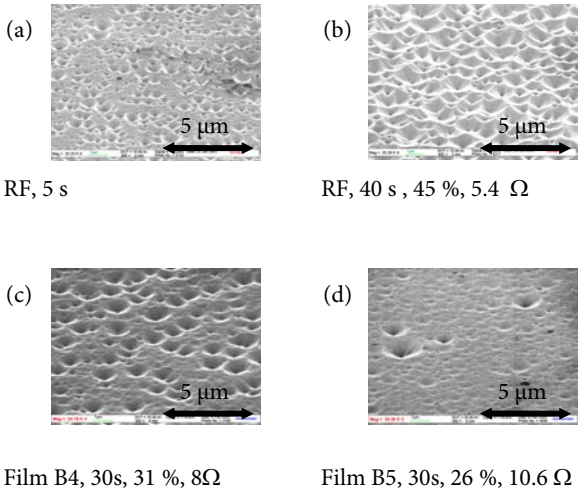

Fig. 5. SEM images of ZnO:Al films after etching in 0.5% HCl. Images (a) and (b) show a reference RF ZnO:Al film etched for varying duration. Images (c) and (d) show films B4 and B5, respectively. Labels below images indicate the respective film type, etch duration, haze at 700 nm and sheet resistance. (See Table 1 for deposition details)

All films when etched for a relatively short time duration of thirty seconds under-went discernable surface texturing. Figures 5 (c) and (d) show the textured surface of films B4 and B5 after etching. It can be seen that for film B4, with F_O = 70 sccm, the film surface has a fair coverage of deep craters with diameters close to 1µm, but when F_O is increased to 80 sccm for B5, craters of this size are considerably less in number. The oxygen distribution thus serves as tool to control the density of points of etch attack. Similar behaviour was observed for series C. Clearly, F_O has an influence on the type of surface structure, after etching, of the ZnO:Al films.

Fig 5 (a) and (b) also demonstrate that once a ZnO:Al film shows a tendency to develop craters of the right shape, their size and thus obtainable haze may be further adjusted within certain limits, by varying the etch duration. Film B2 (PEM = 32.5%, F_O = 60sccm) was etched for 30s, 50s and 70s. As can be seen in Figure 6, the size and number of large craters increased with etching duration. The haze was 20% after 30s etching and increased to a stable value of about 40% as etching duration was increased to 50s and 70s. Comparing the images in Figure 5 (b) and Fig 6 (c) it can be seen that they are remarkably similar in appearance, which suggest, that film B2 is very suitable for light trapping in solar cells.

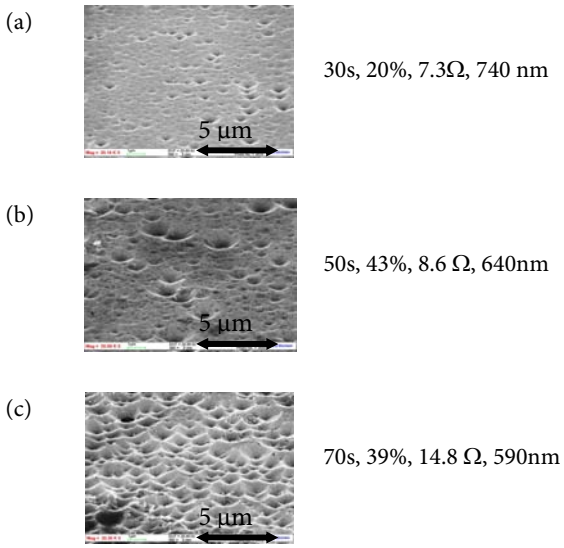

Fig. 6. SEM images of ZnO:Al film type B2 after various etching durations in 0.5% HCl: (a) 30s, (b) 50s, (c) 70s. Labels below each image indicate the respective etch duration, film thickness, sheet resistance and haze ratio at 700nm . (Refer to Table 1 for more details).

3.3.2 Haze Ratio

Another preliminary indication of the light trapping ability of an etched TCO film, is its haze ratio. For conciseness, we consider the haze ratio at an intermediate wavelength (700 nm) to give us a general idea of the light scattering effect. From earlier experiments, the haze ratio at 700 nm, H_{700}, of an etched ZnO:Al film increases as the working point is increased away from the oxide mode to a maximum then drops again as the metallic mode is approached [8]. Similar results were also found for series B and C in our experiments (see figure 7)

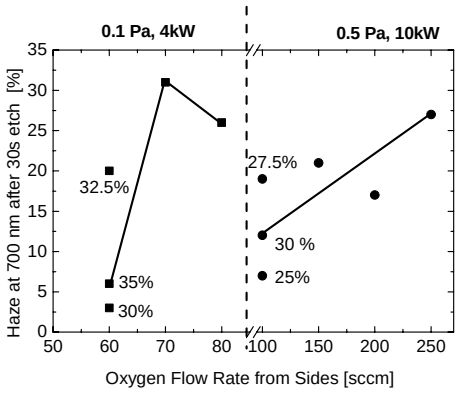

Fig. 7. Haze ratio at 700nm as a function of F_O. Squares and circles represent film types B and C, respectively. All films were etched for 30s in 0.5% hydrochloric acid. See Table 1 for deposition details. Note the lines are to guide the eyes.

Figure. 7 also illustrates a graph of H_{700} after a 30s etch duration, versus F_O at a fixed working point. H_{700} increased

with F_O for series B and C up till 31 % and 27 %, respectively. These values are much higher, than the haze ratios obtained in the simple working point series

3.3.3 Optical Properties of Etched Films

The total transmittance and absorbance spectra of the etched films is shown in figure 8.

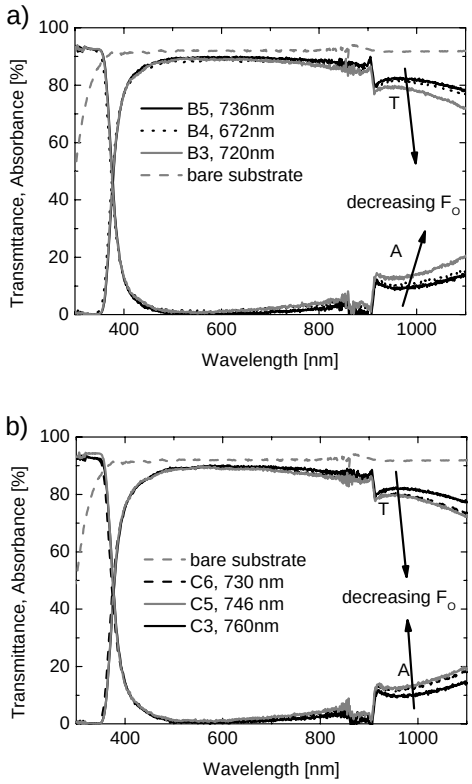

Fig. 8. Total transmittance T, and absorbance A, of etched films prepared with varying amounts of F_O. All films were etched for 30s in 0.5% hydrochloric acid. See Table 1 for deposition details.

The use of CH_2I_2 as an index matching fluid fixed the absorption edge at about 400 nm independently of the band gap energy of the respective ZnO:Al film. The film reflectance is nearly the same (about 10 %) for all films in the wavelength range considered and therefore has not been shown. However, over the visible wavelength, transmittance is close to 90% for all the films and only slightly reduces with decreasing F_O. As the wavelength approaches the NIR range, the reduction in T with decreasing F_O becomes more marked due to increasing absorbance which raises to about 20% at 1100 nm for the lowest value of F_O considered for both film types.

Free carrier absorption must be the cause of this optical behaviour since the increase in absorbance shown in figure 8 coincides with the increase in carrier density (see figure 3).

3.4 Solar Cells

After further optimisation, selected ZnO:Al films were applied as front contacts in 1cm² µc-Si:H solar cells. An optimised RF-sputtered ZnO:Al film was included in each of the cell depositions for both group B and C films as a reference. In all cases, the solar cells using the MF deposited ZnO:Al front contacts achieved higher values of J_{sc} (up to 24.3 mA/cm²) than the RF optimised ZnO:Al (23.2 mA/cm²). The most efficient cell based on MF ZnO:Al had an efficiency of 8.4% which is similar to that of the co-deposited reference cell. The current gain however, could not enhance the efficiency due to the inferior electrical properties of the MF films which lead to lower fill factors of the cells. However, most of the other cells achieved efficiencies of at least 90% relative to the respective reference cell. Note, that the MF ZnO:Al films were deposited at deposition rates as high as 40 nm m/min and 115 nm m/min for low and high power films, respectively. Table 2 shows some solar cell parameters and haze values of the corresponding front contact, for solar cells prepared on the ZnO:Al films of series B and C. In general, the highest values of J_{sc} for the same set of ZnO:Al deposition parameters consistently occurred where the ZnO:Al films had developed a fairly good distribution of large sized craters similar to that of the reference (see Fig 7b). However this is not reflected in the haze value.

Table 2
Solar Cell Parameters for Selected ZnO:Al films

ZnO:Al type	Etch duration [s]	H_{700} [%]	QE at 900nm [%]	J_{sc} [mA/cm²]	η [%]
RF	40	45	26	23.2	8.4
B2	50	43	-	23.9	8.1
B2	70	39	27	24	8.2
B4	30	31	-	23.2	8.2
B4	50	61	27	24.3	8.3
RF	40	45	25	23.1	8.4
C6	50	30	28	24.1	8.2
C6	70	73	29	24.2	8.2
C7	50	24	28	24.3	8.4

Quantum efficiency QE, spectra were determined for the best six cells presented in Table 2. Figure 9 shows the QE results for the µc-Si:H cells on the respective MF deposited ZnO:Al films with the reference cell included for comparison.

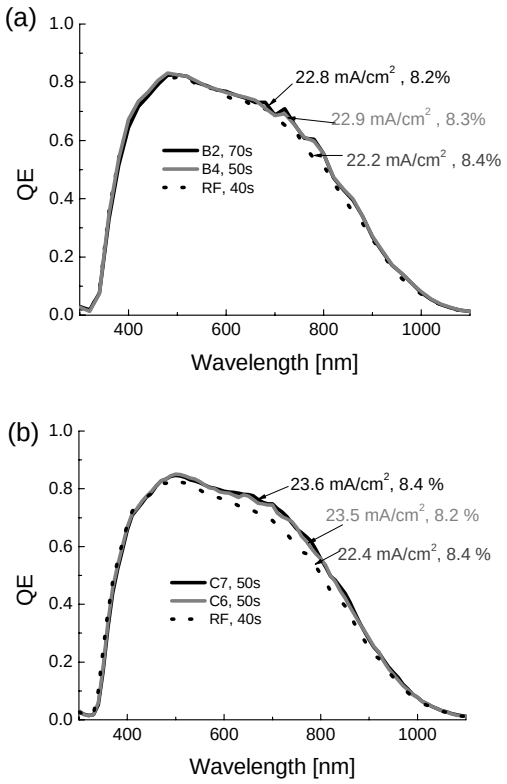

Fig. 9. QE as a function of wavelength for 1 cm² μc-Si:H cells on (a) low power and (b) high power MF ZnO:Al films with the respective reference cells included. The labels indicate J_{sc} calculated from spectral response measurements and the cell efficiency

The increase in J_{sc} was a direct result of improved light trapping leading to an enhancement of QE in the NIR wavelength region. All cells exhibited high QE in the blue and green wavelength region due to the good transmittance of the ZnO:Al films and good index matching of the rough interface. They also exhibited high QE in the red and NIR region, which was a strong indication of their good light trapping ability. The highest J_{sc} for each category of cells was due to a QE at 900nm equal to or exceeding 27 % as can be seen in the fourth column of Table 2.

4. Conclusion

The more uniform distribution of oxygen supply to the MF reactive magnetron sputtering process improves the average resistivity and homogeneity of films deposited in stationary mode. This also possibly contributes to a better structure of films deposited by multi-passes in the dynamic mode. By adjusting the oxygen distribution, we could also prepare favourable surface structure, after etching, for light trapping. The subsequent achievement of short circuit currents above 24mA/cm² and an efficiency of up to 8.4% for a 1 cm² μc-Si:H single junction solar cell further illustrates the benefit of the oxygen inlet modification.

Acknowledgements

This work was supported by the Bundesministerium für Wirtschaft und Technologie (BMWi) under contract No. 0329923A. We are grateful to our colleagues, W. Appenzeller, J. Kirchhoff, W. Reetz and E. Bunte for their contributions. Special thanks also go to H. P. Bochem and E. Brauweiler of Research Centre Jülich for making the SEM images used here. S. Calnan also acknowledges funding by the Engineering and Physical Research Council (EPSRC) through their DTG programme.

References

[1] Müller, J., Schöpe, G., Rech, B., Schade, H., Lechner, P., Geyer, R., Stiebig, H., Reetz, W., Proc. 3rd World Conf. Photovolt. Sol. En. Conversion, Osaka, Japan, 2003, 1839 - 1842

[2] Meier, J., Kroll, U., Dubail, S., Golay, S., Fay, S., Dubail, J., Shah, A., In Proc. 28th IEEE Photovoltaic Specialists Conf., Anchorage, Alaska, 2000, 746 - 749

[3] Groenen, R., Löffler, J., Sommeling, P. M., Linden, J. L., Hamers, E. A. G., Schropp, R. E. I., van de Sanden, M. C. M., Thin Solid Films, 392, 2001, 226 - 230

[4] Löffl, A., Wieder, S., Rech, B., Kluth, O., Beneking, C., Wagner, H., In Proc. 14th European Photovoltaic Solar Energy Conference, Barcelona, Spain, 1997, 2089 - 2092

[5] Rech, B., Müller, J., Repmann, T., Kluth, O., Roschek, T., Hüpkes, J., Stiebig, H. and Appenzeller, W., Materials Research Society, Symposium Proceedings, 762, 2003, A3.1

[6] Rech, B., Schöpe, G., Kluth, O., Repmann, T., Roschek, T., Müller, J., Hüpkes, J., Stiebig, H., Proc. 3rd World Conf. Photovolt. Sol. En. Conversion, Osaka, Japan, 2003, 2783 - 2788

[7] Hüpkes, J., Rech, B., Kluth, O., Repmann, T., Sehrbrock, B., Müller, J., Drese, R., Wuttig, M., 14th Int. Photovoltaic Science and Engineering Conference, Bangkok,. Technical Digest Vol. I, 2004, 379 - 380

[8] Hüpkes, J., Rech, B., Sehrbrock, B., Kluth, O., Müller, J., Bochem, H.P. and Wuttig, M., Proc. 19th European Photovoltaic Solar Energy Conf., Paris, Bd II, 2004, 1415 - 1418

[9] Hüpkes, J., Rech, B., Calnan, S., Kluth, O., Zastrow, U., Siekmann, H., Wuttig, M., Thin Solid Films, In press, Available online 25 August 2005

[10] Szyska, B., Thin Solid Films, 351, 1999, 164 - 169

[11] Strümpfel, J., Beister, G., Schulze, D., Kammer, M., Proc. 40th Annual Tech. Conf. of the Society of Vacuum Coaters, 1997

[12] Kluth, O., Schöpe, G., Hüpkes, J., Agashe, C., Müller, J., Rech, B., Thin Solid Films, 442, 2003, 80 - 85

[13] Tohsophon, T., Hüpkes, J., Calnan, S., Reetz, W., Rech, B., Beyer, W. and Sirikulrat, N. Thin Solid Films, In press, Available online 7 February 2006